



HAL
open science

CEC-normalized clay-water sorption isotherm

W. F. Woodruff, André Revil

► **To cite this version:**

W. F. Woodruff, André Revil. CEC-normalized clay-water sorption isotherm. *Water Resources Research*, 2011, 47, pp.W11502. 10.1029/2011WR010919 . insu-00681819

HAL Id: insu-00681819

<https://insu.hal.science/insu-00681819>

Submitted on 2 Mar 2021

HAL is a multi-disciplinary open access archive for the deposit and dissemination of scientific research documents, whether they are published or not. The documents may come from teaching and research institutions in France or abroad, or from public or private research centers.

L'archive ouverte pluridisciplinaire **HAL**, est destinée au dépôt et à la diffusion de documents scientifiques de niveau recherche, publiés ou non, émanant des établissements d'enseignement et de recherche français ou étrangers, des laboratoires publics ou privés.

CEC-normalized clay-water sorption isotherm

W. F. Woodruff¹ and A. Revil^{1,2}

Received 14 May 2011; revised 8 September 2011; accepted 27 September 2011; published 2 November 2011.

[1] A normalized clay-water isotherm model based on BET theory and describing the sorption and desorption of the bound water in clays, sand-clay mixtures, and shales is presented. Clay-water sorption isotherms (sorption and desorption) of clayey materials are normalized by their cation exchange capacity (CEC) accounting for a correction factor depending on the type of counterion sorbed on the mineral surface in the so-called Stern layer. With such normalizations, all the data collapse into two master curves, one for sorption and one for desorption, independent of the clay mineralogy, crystallographic considerations, and bound cation type; therefore, neglecting the true heterogeneity of water sorption/desorption in smectite. The two master curves show the general hysteretic behavior of the capillary pressure curve at low relative humidity (below 70%). The model is validated against several data sets obtained from the literature comprising a broad range of clay types and clay mineralogies. The CEC values, derived by inverting the sorption/adsorption curves using a Markov chain Monte Carlo approach, are consistent with the CEC associated with the clay mineralogy.

Citation: Woodruff, W. F., and A. Revil (2011), CEC-normalized clay-water sorption isotherm, *Water Resour. Res.*, 47, W11502, doi:10.1029/2011WR010919.

1. Introduction

[2] The development of a unified model for coupled flow in unsaturated clayey materials is needed to model the transport of contaminants in clayey soils and through clay liners, to study the storage of nuclear wastes in argillaceous formations and to understand transport properties in gas shales [Mitchell, 1992; Sammartino *et al.*, 2003; Delay and Distinguin, 2004; Rousseau-Gueutin *et al.*, 2010; Jougnot *et al.*, 2010; Schneider and Goss, 2011]. We have recently developed a unified set of constitutive equations for the transport of ionic species in clay materials [Revil *et al.*, 2011]. The extension of this theory to the unsaturated case requires a precise analysis of the water retention curves in these materials, especially the clay-water sorption isotherms at low relative humidity (below 70%).

[3] According to Saarenketo [1998], Aochi and Farmer [2010], and Conin *et al.* [2011], the pore water in clay materials can be divided into two important categories (1) hygroscopic water and (2) capillary and free waters. In the present paper we are especially interested in the sorption and desorption of the hygroscopic water. The hygroscopic (sorbed) water on the surface of a clay mineral is classically seen as consisting of (1) a monomolecular layer mainly located around the negatively charged mineral surface sites (with an approximate thickness of 2 nm) and (2) additional water molecules loosely bound to the mineral surface with a thickness on the order of 4 nm [Saarenketo,

1998]. This kind of multilayer model is the basis for several empirical relationships used in modeling sorption isotherms [see Cancela *et al.*, 1997; Furmaniak *et al.*, 2005; Limousin *et al.*, 2007] in addition to physically based sorption models (e.g., Tuller and Or [2005]). In the case of smectite, the hydration sequence is often described by the intercalation of one, two, and less commonly three water layers leading to the individualization of hydration steps on water sorption curves corresponding to zero, one, and two water sheets in the interlayer. Deviation from this representation is usually associated with (1) hydration heterogeneity, i.e., the interstratification of layers with different hydration states that smoothens the sorption curve and (2) capillary sorption in pore network at high relative humidity [Cases *et al.*, 1997; Bérend *et al.*, 1995; Ferrage *et al.*, 2005; Michot *et al.*, 2005; Ferrage *et al.*, 2010; Malikova *et al.*, 2007].

[4] This uniform layer model is challenged, however, by other researchers. For instance Laird [1999] suggested that instead of a uniform film, the water molecules are clustered around cation/charge sites. This implies that the cation exchange capacity, rather than the specific surface area, should be used to normalize clay-water sorption isotherms.

[5] Clay-water sorption and desorption isotherms define the relationship between the water content and the relative humidity at a prescribed temperature and effective pressure. For clay minerals, the water content is given as the mass of water per gram of dry clay plotted as a function of the water activity (relative humidity). This water activity is defined as the ratio of the partial pressure of water to the saturation vapor pressure of the water phase. Sorption isotherms are observed to be hysteretic [Cancela *et al.*, 1997; Likos and Lu, 2002; Shang *et al.*, 1995]. The amount of sorbed water in a given clay is known to be influenced by the texture of the clay material and therefore by its

¹Department of Geophysics, Colorado School of Mines, Golden, Colorado, USA.

²ISTerre, CNRS, UMR CNRS 5275, Université de Savoie, Le Bourget du Lac, France.

mineralogy [Stepkowska *et al.*, 2004; Newman, 1983; Rinnert *et al.*, 2005] and by the specific metal ion sorbed in the Stern layer, the inner layer of the electrical double layer [Salles *et al.*, 2009; Dontsova *et al.*, 2004; Montes-Hernandez *et al.*, 2003; Cancela *et al.*, 1997].

[6] The classical Brunauer, Emmett, and Teller (BET) theory recognizes the strong correlation between the specific surface area and monolayer sorption of water (see the de-Boer *t*-curve approach and its application [Kowalczyk *et al.*, 2005]). In the present paper we develop a normalized clay-water sorption isotherm by using the CEC of the clay material as a normalizing parameter. Saarenketo [1998] showed, for instance, that the dielectric constant of a clayey material is both correlated to the amount of water sorbed per unit weight of dry clay and to the CEC. The CEC is observed to be linearly related to the specific surface area of clay minerals [Newman, 1983; Revil *et al.*, 1998; Srodon and McCarty, 2008; Salles *et al.*, 2009; Conin *et al.*, 2011] (see Figure 1). In addition, because of the clustering of the water molecules around the cations/charge sites, we suggest that the CEC of the mineral can be used as a better surrogate for the specific surface area in a normalized model, enabling the prediction of the clay-water sorption isotherm (including the hysteresis loop) from a single pair of master curves in the low relative humidity range (more precisely at low

thicknesses of surface-sorbed water corresponding to one or two monolayers). The significant linear correlation between CEC, specific surface area, and hygroscopic water content has been shown earlier for soils [e.g., Banin and Amiel, 1970; Smith *et al.*, 1985; Yukselen-Askoy and Kaya, 2010]. Therefore, it is evident that a similar model based on specific surface area normalized sorption may yield a similar master “water-retention curve.” We will discuss the advantages of using the CEC instead of the specific surface area as the normalizing parameter in section 4.

2. Background

[7] In section 2, we discuss the relationships between the cation exchange capacity (CEC), the specific surface area, and the density of sorbed water molecules in clay materials.

2.1. The Cation Exchange Capacity (CEC)

[8] The CEC represents the capacity of a porous material (generally a soil) to exchange cations (generally Ca, Mg, K, and Na) between the mineral surface and the pore water solution. It is generally measured at pH 7 [Carroll, 1959]. The pH dependence of the CEC can only be understood in terms of the electrical double layer attached to the mineral surface. In SI units, the CEC is expressed in $C\ kg^{-1}$, but is classically expressed in $meq\ g^{-1}$ (with $1\ meq = 1\ mmol$ equivalent charge, e.g., $1 \times 10^{-3} e N$, where $e = 1.6 \times 10^{-19} C$ and N is the Avogadro constant, $6.022 \times 10^{23} mol^{-1}$). For clay mixtures, the average CEC is determined from the respective exchange capacities of the constituent clay types. For example, the cation exchange capacity of a mixture of kaolinite, illite, and smectite is given by [Rabaute *et al.*, 2003]

$$CEC = \chi_K CEC_K + \chi_I CEC_I + \chi_S CEC_S, \quad (1)$$

where χ_i represents the mass fraction of mineral *i*, and K, I, and S stand for kaolinite, illite, and smectite, respectively. Equation (1) is scaled by the mass fraction of the clay minerals φ_w , which can be obtained by XRD analysis. Equation (1) can be adapted to clayey sands and sandstones by neglecting the CEC associated with the silica grains [Rabaute *et al.*, 2003].

[9] The CEC is also linearly correlated to the specific surface area S_{Sp} (in $m^2\ g^{-1}$) of the mineral grains [Patchett, 1975; Revil *et al.*, 1998; Revil and Leroy, 2004; Yukselen and Kaya, 2006],

$$CEC = Q_S S_{Sp}, \quad (2)$$

where Q_S ($C\ m^{-2}$) is the surface charge density of the clay fraction, which is related to the total excess of electrical charge per unit pore volume Q_V (expressed in $C\ m^{-3}$) as $Q_S = Q_V(S/V_p)^{-1}$, where S is the surface area of the mineral grain and V_p represents the pore volume (see Figure 1). Figure 1 shows the linear data trend for the specific surface area S_{Sp} (in $m^2\ kg^{-1}$) as a function of the CEC. Revil *et al.* [1998] and Revil and Leroy [2004] obtained an equivalent charge density comprised between 1 to 3 charges per nm^2 at pH 7 with an average surface charge density of 2 elementary charges per nm^2 (Figure 1).

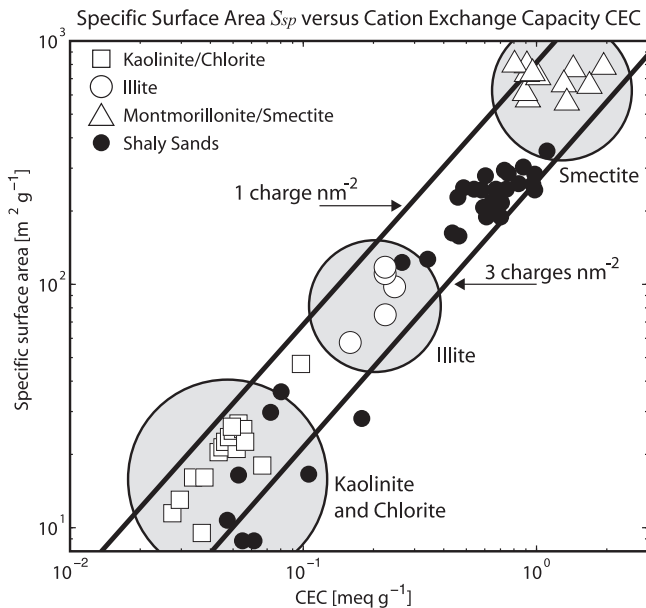


Figure 1. Specific surface area of clay minerals (in $m^2\ g^{-1}$) as a function of the (absolute) (in $meq\ g^{-1}$ with $1\ meq\ g^{-1} = 96,320\ C\ kg^{-1}$ in SI units) for various clay minerals. The ratio between the CEC and the specific surface area gives the equivalent total surface charge density of the mineral surface. Generalized regions corresponding to kaolinite, illite, and smectite are represented by shaded circles. Figure adapted from Revil and Leroy [2004]. The two lines corresponds to one to three elementary charges per unit surface area. Data from Patchett [1975], Lipsicas [1984], Zundel and Siffert [1985], Lockhart [1980], Sinitsyn *et al.* [2000], Avena and De Pauli [1998], Shainberg *et al.* [1988], Su *et al.* [2000], and Ma and Eggleton [1999].

[10] The type of crystalline planes at the mineral water interface varies considerably among clay types. A sketch of two representative end members, kaolinite and smectite, is provided in Figure 2. Despite the complex crystalline structure of clay minerals, the properties of clays and shales (like the surface electrical conductivity) depend mainly on macroscopic parameters like the specific surface area and the CEC. In the water sorption case, this indicates that the sorption heats are generally independent of the type of crystalline planes and can be therefore similar for clays of different mineralogy.

[11] The specific surface area can be obtained from water sorption isotherms by estimating the cross-sectional area of a water molecule ε (typically $\varepsilon \approx 12 \text{ \AA}^2$ per molecule, see Middleton [2003]). Salles *et al.* [2009] use the following relationship to determine the specific surface area of a clay material from water sorption isotherms:

$$S_{\text{Sp}} = \varepsilon n_m M_w, \quad (3)$$

where n_m denotes the number of water molecules sorbed in a monolayer (in mol) and M_w is the molar mass of water (kg mol^{-1}). It follows that the specific surface area can be obtained from the mass fraction of water in the sample during the first stage of sorption assuming, like the BET theory, that water sorbs by first filling a monolayer (no

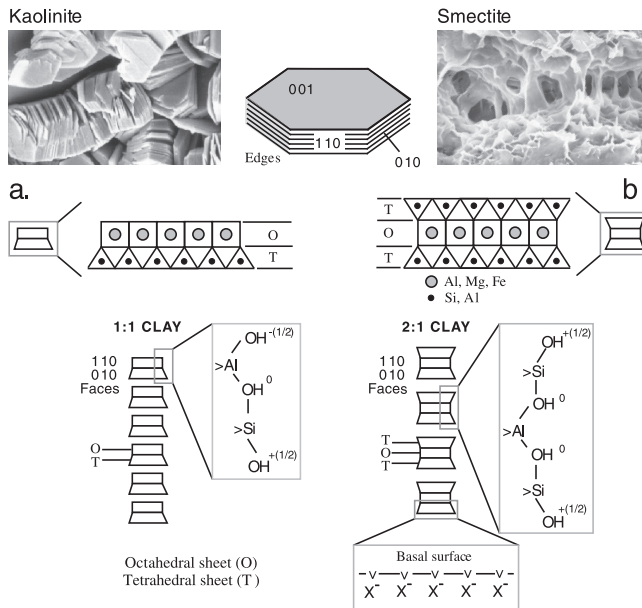


Figure 2. Active surface sites at the edge of (a) 1:1 clays (e.g., kaolinite) and (b) 2:1 clays (e.g., smectite or illite). In the case of kaolinite, the surface sites are located primarily on the edge of the mineral grain ($\{110\}$ and $\{010\}$ planes). In the case of smectite and illite (in the pH range near neutrality, 5 to 9) the surface sites are predominantly located on the basal plane ($\{001\}$ plane) and they are due to isomorphous substitutions inside the crystalline framework. Note the difference in the morphology of the clay particles and the variety of crystallographic planes. The letters T and O represent tetrahedral and octahedral sheets, respectively. Adapted from Leroy and Revil [2009].

local condensation of packs of water molecules). However, this is a vast simplification, because capillary condensation on rough particle surfaces and clustering of water molecules around charge sites can be important. In addition, water sorption is also correlated to the ionic potential of the exchangeable cation sorbed on the active mineral surface sites present on different crystalline planes (see Figure 2) [Dontsova *et al.*, 2004; Salles *et al.*, 2009].

[12] As discussed above, the CEC is an average parameter describing the sorption of counterions on the surface of the clay grains. The reality is, however, more complex: different crystalline planes, with different electrochemical characteristics, contribute to complex sorption behavior. For instance, a bivalent ion like Cu^{2+} can form both monodentate and bidentate complexes with the clay surface. For silica, the former occurs as an inner sphere ligand, and the latter occurs as an outer sphere ligand [Vaudelet *et al.*, 2011a, 2011b]. To account for this complexity, we introduce an empirical scaling parameter δ_i that depends only on the exchangeable cation i and is independent of the clay type. This parameter is used to scale the measured cation exchange capacity with a given cation i as

$$\overline{\text{CEC}}_i = \delta_i \text{CEC}, \quad (4)$$

where $\overline{\text{CEC}}_i$ is a value of the cation exchange capacity for ionic species i , while CEC is the absolute cation exchange capacity. The absolute cation exchange capacity is measured using a cation that has a very strong affinity with the mineral surface (like ammonium or cobalt); it corresponds to the cation exchange capacity reported in Figure 1. Other cations always have affinities smaller than the cations used to measure the absolute cation exchange capacity; therefore, $\delta_i \leq 1$ and $\overline{\text{CEC}}_i \leq \text{CEC}$. A description of the empirical analysis performed to constrain the scaling parameter δ_i is provided below in section 2.4. The following set of values will be discussed below in section 2.4: $\delta(\text{Li}) = 0.4$, $\delta(\text{Na}) = 0.5$, $\delta(\text{Mg}) = 0.6$, and $\delta(\text{Ca}) = 0.8$. The scaling parameter δ_i reflects the affinity of the cations for the mineral surface (i.e., the parameter is equal to one for cobalt and ammonium).

2.2. Relative Humidity and Water Content

[13] For the nonhygroscopic water and at thermodynamic equilibrium, the capillary pressure P_c (in Pa) is classically defined as the pressure differential between the fluid and vapor pressures across an interface by the Young-Laplace equation,

$$p_c = \frac{2\gamma \cos \theta}{r}, \quad (5)$$

where γ denotes the surface tension (N m^{-1}), θ the wetting angle (in rad), and r the effective radius of the meniscus between the two phases (in m). Capillary pressure depends on the saturation of the wetting phase and the saturation/desaturation history in the porous material, and is defined as the difference of the pressures of the wetting (index w) and nonwetting (index n) phases,

$$P_c = P_n - P_w. \quad (6)$$

The change in vapor pressure due to the shape of the meniscus with radius r is given by the Kelvin equation

$$RT \ln \left(\frac{p_v}{p_v^0} \right) = \frac{2\gamma M_V}{r}, \quad (7)$$

where M_V ($\text{m}^3 \text{mol}^{-1}$) is the molar volume of water, p_v^0 is the vapor pressure of the reference state (saturated vapor pressure), $R = 8.31 \text{ J K}^{-1} \text{ mol}^{-1}$ is the universal gas constant, and T is the absolute temperature (in Kelvin). The saturation vapor pressure is given by [Likos and Lu, 2002; Jougnot et al., 2010]

$$p_v^0 = p_v^{\text{sat}}(T) = 10^{f(T)}, \quad (8)$$

$$f(T) = a + (T - T_0)[b + c(T - T_0)], \quad (9)$$

where the superscript "0" indicates the saturated reference state ($p_c = 0$, $p_w = p_w^0 = p_{\text{atm}}$), $T_0 = 273.5 \text{ K}$, $a = 2.7858$ (dimensionless), $b = 31.559 \text{ K}$, $c = 0.1354$ (dimensionless).

[14] The relative humidity h_r (given usually in %) (alternatively, the water activity p_v/p_v^0) can be related to the pressure of the water phase by [Shang et al., 1995]

$$h_r = \frac{p_v}{p_v^0} = \exp \left[\frac{M_v}{RT} (p_w - p_w^0) \right]. \quad (10)$$

The connection between the volumetric or gravimetric water content associated with the adsorption of water molecules onto a charged mineral surface and the water saturation S_w is easily established. The volumetric water content θ is defined as the ratio of the volume of water V_w to the total volume of the medium V_T ; porosity ϕ is defined as the ratio of the void volume V_v to the total volume V_T ; water saturation, V_w/V_v , can be written as

$$S_w = \frac{\theta}{\phi}. \quad (11)$$

Water saturation can also be obtained from the gravimetric water content v (dimensionless). The gravimetric water content represents the mass of water divided by the mass of mineral grains. It is normally measured by taking the weight of a moist sample and the weight of a dried sample of the same material, which yields $\theta = v \rho_{\text{dry}} / \rho_w$, where $\rho_{\text{dry}} = (1 - \phi) \rho_g$ represents the mass density of the dry porous material, ρ_g the mass density of the grains (typically 2600 to 2800 kg m^{-3}), and ρ_w the density of the pore water (all in kg m^{-3}). Using this relationship together with equation (11) yields

$$S_w = \frac{1 - \phi}{\phi} \frac{\rho_g}{\rho_w} v. \quad (12)$$

2.3. Modeling Water Sorption Isotherms

[15] Sorption isotherms represent the retention and/or release of liquid compounds on a solid interface [Limousin et al., 2007]. Numerous empirical and mechanistic models have been developed to characterize sorption phenomena, resulting in several general isotherm types [Brunauer et al.,

1938; Broekhoff and Boer, 1967a; Gauden, 2005; Limousin et al., 2007], which have been empirically validated in the literature for macroscopic phenomenology and simplified microscale geometries [see Broekhoff and Boer, 1967b; Cancela et al., 1997; Neimark and Ravikovitch, 2001; Ravikovitch and Neimark, 2002; Furmaniak et al., 2005]. Water sorption isotherms in clayey materials are generally characterized by sigmoidal curves, marked by a point of inflection between the minimum and maximum values. We will show later that this point of inflection corresponds to the saturation of the first layer of sorbed water on the mineral surface.

[16] A classical model describing the sorption of a gas (like nitrogen) on a reactive mineral surface is the Brunauer, Emmett, and Teller (BET) model [Brunauer et al., 1938]. This theory has been extended to the case of water vapor sorption in clays [Mooney et al., 1952; Chemkhi et al., 2004; Mihoubi and Bellagi, 2006]. The BET theory is an extension of the Langmuir theory for a monolayer molecular adsorption. Assuming the formation of several layers for molecular sorption with no interaction between the layers, the BET equation is written as [e.g., Cancela et al., 1997]

$$\frac{1}{v \left(\frac{1}{h_r} - 1 \right)} = \frac{C - 1}{v_m C} h_r + \frac{1}{v_m C}, \quad (13)$$

where v represents gravimetric water content discussed above and $v_m = n_m M_w / m_g$ (dimensionless) represents the gravimetric water content when the first monolayer is fully saturated, i.e., the monolayer adsorbed water mass $n_m M_w$ per mass of the grains m_g , where M_w is the molar mass of water in kg mol^{-1} ($18.02 \times 10^{-3} \text{ kg mol}^{-1}$) and n_m denotes the number of water molecules sorbed in a monolayer (expressed in mol). The so-called BET constant C is an energetic term representing the balance of adsorption energies at constant temperature,

$$C = \exp \left(\frac{E_a - E_l}{RT} \right), \quad (14)$$

where E_a is the heat of adsorption of the first layer of water molecules covering the clay surface, E_l is the heat of adsorption for the second and third layer of water molecules covering the mineral surface and is equal to heat of water liquefaction, R is the molar gas constant ($8.31 \text{ J mol}^{-1} \text{ K}^{-1}$), and T is temperature (in K). Using equations (10) and (13) the BET equation can be rewritten as

$$\frac{h_r}{v(1 - h_r)} = \frac{C - 1}{v_m C} h_r + \frac{1}{v_m C}. \quad (15)$$

The term of this equation can be arranged as follows:

$$v = v_m \left(\frac{h_r}{1 - h_r} \right) \left[\frac{C}{(C - 1)h_r + 1} \right]. \quad (16)$$

We will normalize this curve by the cation exchange capacity to produce new master curves in section 2.4.

2.4. A Normalized Sorption Curve Model

[17] For the purposes of this derivation, the two quantities v and v_m will be expressed in grams of water per gram of dry solid rather than in m^3 . The mechanisms governing water sorption in a clay matrix change as a function of water content. At both low and high water activities, sorption isotherms exhibit highly variable and nonlinear character. At low water activity, nonlinear effects may be due to local condensation of the water molecules due to the roughness of the mineral/water interface. At high water activity (above 0.61, see below in section 3.2), capillary effects start to dominate. However, for a wide range of water activities (e.g., $h_r \equiv p_v/p_v^0 \in [0.05, 0.70]$), the isotherms exhibit a reproducible character that is consistent across a diverse set of clay types [Salles *et al.*, 2009; Cancela *et al.*, 1997; Likos and Lu, 2002]. This is a consequence of the fact that vapor sorption in this regime is driven by the interaction of water molecules with the surface of the negatively charged clay particles (at pH 7).

[18] As discussed in section 2.1, the CEC is a measure of the amount of exchangeable charge per unit mass of the solid. It is directly related to the specific surface area S_{Sp} of the clay (Figure 1). As such, the CEC can be used to scale the sorption isotherms measured for different clays, effectively collapsing the various, respective isotherms into a single master curve corresponding to the water sorption equivalent v/CEC (expressed in g meq^{-1} , gram of water per milliequivalent) as a function of the activity of the fluid phase (relative humidity). By simply normalizing equation (15) by the CEC, we obtain an equivalent sorption isotherm that is valid for individual subsets of clays,

$$\frac{v}{\text{CEC}} = \frac{v_m}{\text{CEC}} \left(\frac{h_r}{1-h_r} \right) \left[\frac{C}{(C-1)h_r + 1} \right]. \quad (17)$$

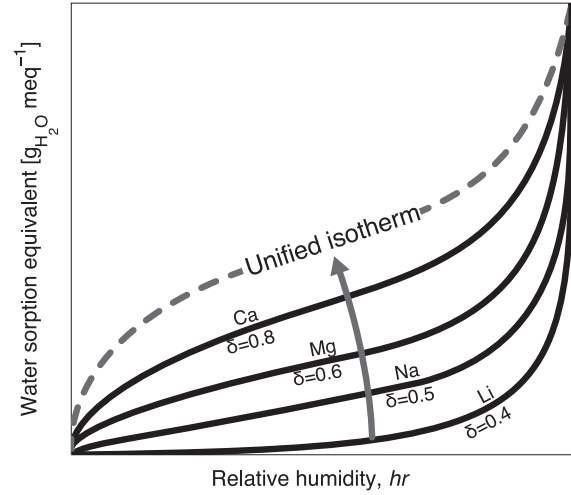
[19] According to equation (15), the relationship between the BET parameter $h_r/[v(1-h_r)]$ and the relative humidity h_r is a line with a slope $(C-1)/(Cv_m)$. Recognizing that the slope for the normalized isotherm must be the same for all clay types, we redefine the CEC-normalized BET monolayer sorption constant as $v_m^{\text{CEC}} = v_m/\text{CEC}$ and the slope parameter from equation (15) as $\xi = (C-1)/(Cv_m^{\text{CEC}})$. Hence, the BET constant can be written in terms of the slope parameter as $C = (1 - \xi v_m^{\text{CEC}})^{-1}$. From these considerations, we obtain a master equation for the CEC-normalized sorption model,

$$\frac{\text{CEC}}{v} \left(\frac{h_r}{1-h_r} \right) = \frac{1}{v_m^{\text{CEC}}} + \xi(h_r - 1). \quad (18)$$

[20] To account for different types of cations sorbed on the mineral surface, we introduced a scaled-CEC parameter $\overline{\text{CEC}}_i$, defined by equation (4) above. For the sake of clarity, this parameter effectively replaces the CEC in equations (17) and (18) and has been determined empirically from the data analysis presented below in section 3. The effect of this parameter is illustrated in Figures 3 and 4 where we show that adopting the normalization by the scaling parameter δ_i collapses all the sorption curves into a master curve. This yields the following normalized sorption isotherm;

$$\frac{1}{v} \left(\frac{h_r}{1-h_r} \right) = \frac{1}{\bar{v}_m} + \bar{\xi}(h_r - 1), \quad (19)$$

a. Affect of δ on CEC-normalized sorption isotherms



b. Affect of δ on CEC-normalized BET lines

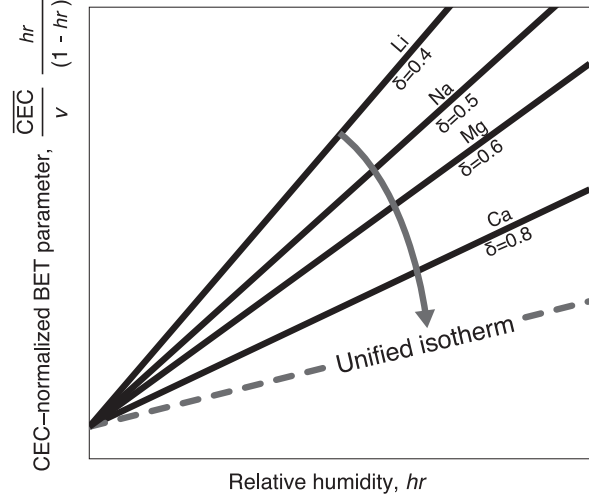


Figure 3. The effect of the mineralogical parameter δ on CEC-normalized isotherms comprising clays of different subsets. (a) Sorbed water content. (b) BET-normalized linear trends. For clays of similar mineralogy with the same surface hydration energy, i.e., exchanged counterion, CEC-normalized isotherms correspond to several characteristic equivalent curves shown as black lines. Scaling the respective CEC values by δ_i (counterion dependent) collapses these curves into a single normalized model.

where the two normalized parameters are defined as

$$\bar{v} = v/\overline{\text{CEC}}_i, \quad (20)$$

$$\bar{v}_m \equiv v_m/\overline{\text{CEC}}_i, \quad (21)$$

$$\bar{\xi} \equiv (C-1)/(C\bar{v}_m). \quad (22)$$

[21] To constrain the value of the scaling parameter δ_i for a selection of ions i , montmorillonite and bentonite

pairs were selected from the works of *Cancela et al.* [1997] and *Montes-Hernandez et al.* [2003]. Separate inversions of CEC values were performed for the respective Ca, Li, and Mg-exchanged members of these two data sets. As the model predicts, each subset collapses to a unique CEC-normalized trend. The resulting CEC values were compared with the output of the values of \overline{CEC}_i obtained from

the inversion of the complete data set to estimate the corresponding δ_i values for these three subsets. Figure 4 shows the results of this analysis, further validating our conceptual model.

[22] Water sorption in porous media almost ubiquitously exhibits hysteresis. This behavior may arise from any of the following effects: (a) capillary condensation, (b) changes in clay morphology, (c) effects of pore topology in which the filling and emptying pathways differ [*Dontsova et al.*, 2004], and (d) contact angle dynamics on chemically heterogeneous and rough surfaces [*Tuller and Or*, 2005]. The general character of hysteresis in the wetting/drying loop is such that the desorption isotherm exhibits higher water content than its adsorption counterpart at the same relative humidity. Indeed, there is some variability observed in the hysteresis, which may indicate the cumulative influence of the aforementioned affects in sequential experiments [see *Aochi and Farmer*, 2010]. The present model accounts for hysteresis by considering all mechanisms contributing to the retention of additional water in the drying loop as “bound water” bw represented by an empirical constant $\Gamma = bw/\overline{CEC}_i$ of the same dimensionality as the water content (i.e., g g^{-1} or mmol g^{-1}). This term is added to the normalized monolayer parameter \bar{v}_m in our present formulation. Hence we reparameterize equation (18) to arrive at a formulation of master curves for the normalized sorption/desorption model,

$$\frac{1}{v} \left(\frac{h_r}{1-h_r} \right) = \frac{1}{\bar{v}_m + \Gamma} + \bar{\xi}(h_r - 1). \quad (23)$$

Although equation (19) has been derived from BET theory, similar relationships can be obtained by the same reasoning for other models of clay-water sorption isotherms. Equation (23) is the main equation derived in our paper. It will be tested in the next section using a variety of literature data.

3. Validation of the Model

[23] The model, equation (23), was applied to data taken from the literature. We first apply the model to desorption data obtained for Na-exchanged kaolinite-smectite mixtures. The data set is then expanded to include additional water sorption measurements in a variety of clays including kaolinite, smectite, montmorillonite, and bentonite, comprising a diverse array of exchangeable cations for these clays (see Tables 1 and 2 for the appropriate references). To mitigate the effect of temperature on the present analysis, data were selected only from data sets collected at temperatures ranging from 20 to 30°C. The influence of temperature will be evaluated further below in section 3.4, and we will see that this assumption is well justified. Thermodynamic analysis indicates that temperature variation on the order of 10°C produces comparable water retention characteristics in clays [*Schneider and Goss*, 2011].

3.1. Sorption Isotherms in Na-Exchanged Kaolinite-Smectite Mixtures

[24] *Likos and Lu* [2002] conducted experiments to measure water adsorption as a function of the clay fraction of respective kaolinite-smectite mixtures. Pure kaolinite and smectite end members were slurry mixed to achieve

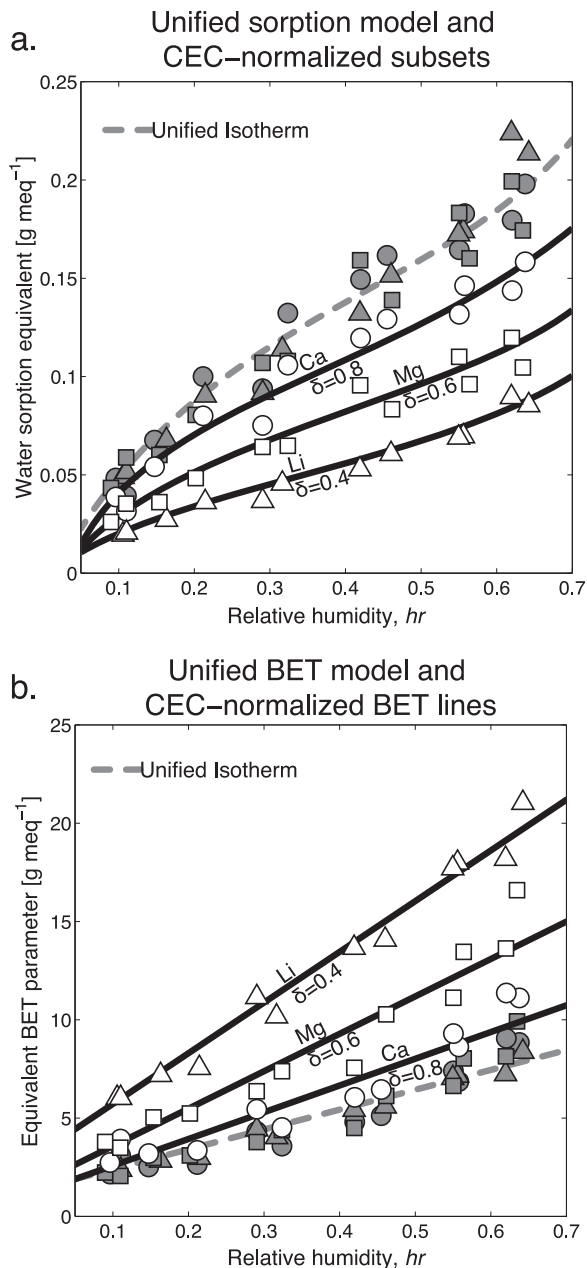


Figure 4. CEC values were inverted independently for three clay subsets comprising the Ca, Li, and Mg members of separate montmorillonite and bentonite data sets. The CEC-normalized data define three unique curves, which collapse to a normalized curve when scaled by the normalized cation exchange capacity \overline{CEC}_i . (a) Water content. (b) Equivalent BET-parameter straight lines. In both cases, the dashed line corresponds to the normalized isotherm. Data from both *Cancela et al.* [1997] and *Montes-Hernandez et al.* [2003].

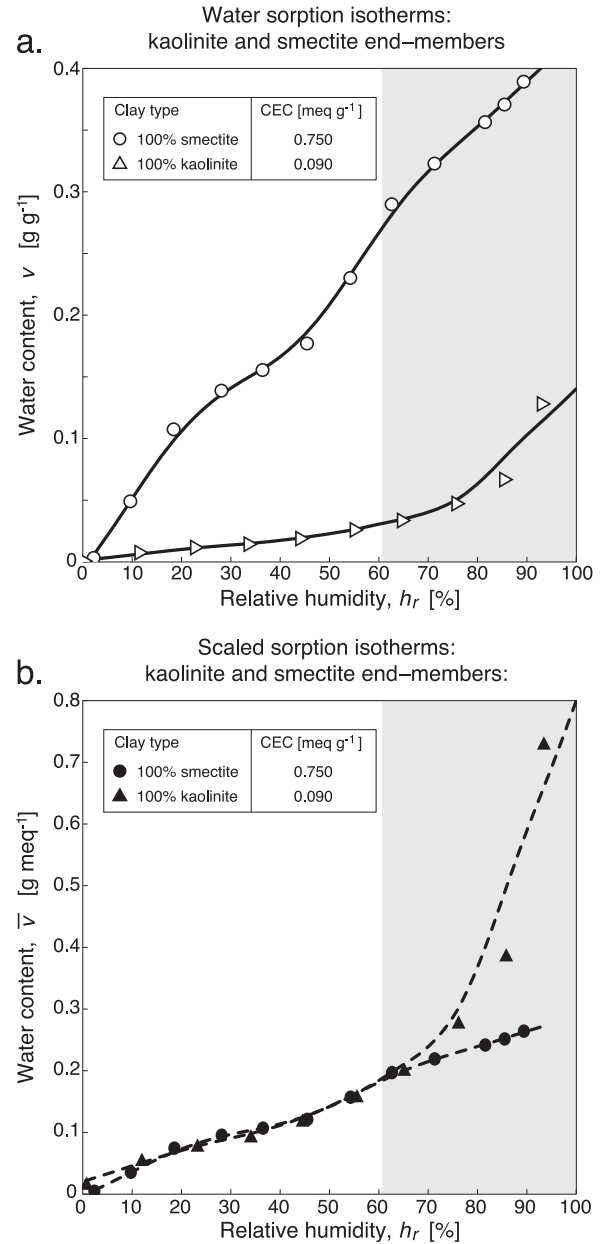
Table 1. Data Sets Used in the Analysis and Corresponding Citations for the Adsorption Data

Clay Type	Citation
Ca-Montmorillonite	<i>Cancela et al. [1997]</i>
Cu-Montmorillonite	
Fe-Montmorillonite	<i>Krushin [2005]</i>
Li-Montmorillonite	
Mg-Montmorillonite	
Na-Montmorillonite	
Shale-A (Na)	
Shale-C (Na)	
Shale-D (Na)	
MidwayShale (Na)	
Bentonite (Al-Fe-Mg-Na-Ca-K)	
Bentonite (Ti-Al-Fe-Mn-Mg- Ca-Na-K-P)	
Ca-Bentonite	<i>Montes-Hernandez et al. [2003]</i>
K-Bentonite	
Li-Bentonite	
Mg-Bentonite	<i>Mihoubi and Bellagi [2006]</i>
Na-Bentonite	
Raw-Bentonite (Na/Ca)	
Sapponite (Al-Mg-Na)	
	<i>Mokrejš et al. [2005]</i>
	<i>Montes-Hernandez et al. [2003]</i>
	<i>Rinnert et al. [2005]</i>

mass-controlled clay ratios of 20%, 50%, 70%, 80%, and 90% smectite. Vapor desorption isotherms were then determined for each composite clay type for h_r ranging from 0% to 95%. The theory presented in section 2 is applied to the data as a first-order verification of the proposed model. The sorption isotherms were normalized by estimated CEC values for the end-member specimens, as well as for all of the clay mixtures, showing promising results (see Figures 5 and 6).

Table 2. Data Sets Used in the Analysis and Corresponding References for the Desorption Data

Clay Type	Citation	
Wyoming montmorillonite (Na)	<i>Krushin [2005]</i>	
Wyoming smectite, SWy-1 (Na)		
Wyoming montmorillonite, Clay Spur (Na)	<i>Likos and Lu [2002]</i>	
MX-80 Bentonite, Wyoming (Na)		
Natural Volclay, Wyoming bentonite (Ca-Mg-Na)		
Natural Volclay, Wyoming bentonite (Na)		
Shale-A (Na)		
Shale-C (Na)		
Shale-D (Na)		
100% Smectite (Na)		
100% Kaolinite (Na)		
10/90 Kaolinite-Smectite (Na)		
20/80 Kaolinite-Smectite (Na)	<i>Mihoubi and Bellagi [2006]</i>	
30/70 Kaolinite-Smectite (Na)		
50/50 Kaolinite-Smectite (Na)		
80/20 Kaolinite-Smectite (Na)		
Bentonite (Al-Fe-Mg-Na-Ca-K)		
Bentonite (Ti-Al-Fe-Mn-Mg- Ca-Na-K-P)		
Ca-Bentonite		<i>Montes-Hernandez et al. [2003]</i>
K-Bentonite		
Li-Bentonite		
Mg-Bentonite		<i>Rinnert et al. [2005]</i>
Na-Bentonite		
Raw-Bentonite (Na/Ca)		
Sapponite (Al-Mg-Na)		
Soil-716	<i>Schneider and Goss [2011]</i>	

**Figure 5.** Preliminary inversion. (a) Raw adsorption isotherms. (b) CEC-normalized sorption isotherms for the kaolinite and smectite end members. The shaded gray region represents the saturation regime in which capillary effects begin to dominate vapor sorption in the clays, causing a departure from the normalized model. CEC values for used for the normalization are also shown.

[25] CEC values were inverted using a stochastic inversion algorithm based on an MCMC approach called the adaptative metropolis algorithm (AMA [see Haario et al., 2001; Woodruff et al., 2010, and references therein], see discussion in Appendix A). The resulting CEC values and the normalized sorption isotherm for these clays are provided in Figure 7. In Figure 7b we plot the inverted CEC (determined from the peak of the posterior probability densities) as a function of the clay content. We see that the CEC of the two end members (kaolinite and smectite) are

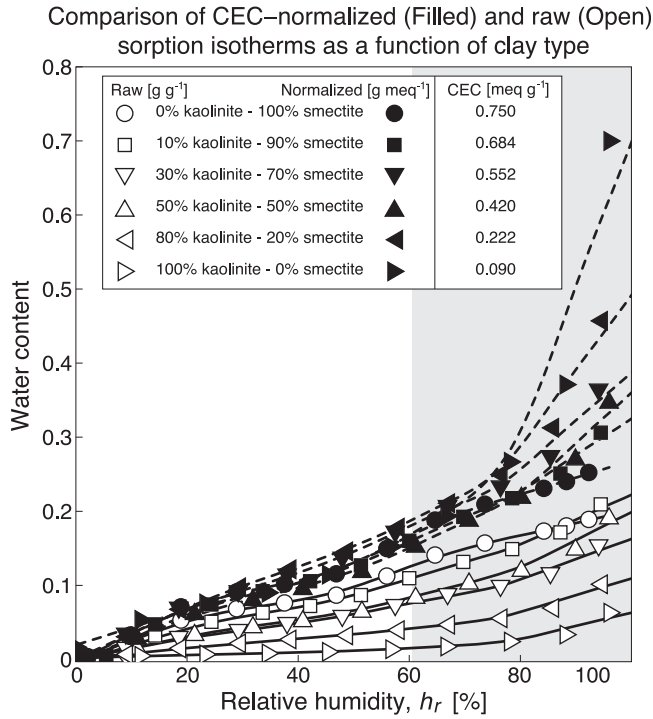


Figure 6. Comparison of raw (open) and CEC-normalized (filled) data using estimated values for the CEC. The shaded region represents the saturation regime in which vapor desorption is dominated by capillarity, causing a departure from the proposed model. Data from *Likos and Lu* [2002].

consistent with the range of CEC values for these two clays (see Figure 1). Also the inverted CEC of a given mixture is consistent with a linear mixture model [see equation (1), $CEC(\text{mixture}) = \chi_K CEC_K + (1 - \chi_K) CEC_S$, where χ_K is the relative mass fraction of kaolinite and CEC_K and CEC_S represent the CEC of the two end members, kaolinite and smectite, respectively).

3.2. Application of the Normalized Model

[26] The procedure outlined in section 3.1 was repeated for the expanded data set. However, the data were inverted for the scaled exchange parameter \overline{CEC}_i instead of the CEC. A comparison of the raw data to the inverted data (scaled by \overline{CEC}_i) is presented in Figure 8. This \overline{CEC}_i -normalized data set was then used to invert the normalized monolayer water content \bar{v}_m , the normalized BET energy constant $\bar{\xi}$, and the bound water parameter Γ , which define the normalized sorption curve. The normalized data and the corresponding model fit are shown in Figures 9 and 10 (see Appendix A for the explanations regarding the optimization scheme used in this analysis). The normalized isotherm accurately fits the data fairly well. It captures the wetting/drying hysteresis exhibited by the data (Figure 11). It also provides a model applicable to clays, sand-clay mixtures, and sandstones. The results of the inversion are reported in Tables 3 and 4.

[27] For this analysis, the energy constant was allowed to differ for adsorption and desorption, implying that the difference in sorption heats $\Delta E = E_a - E_l$ (see equation

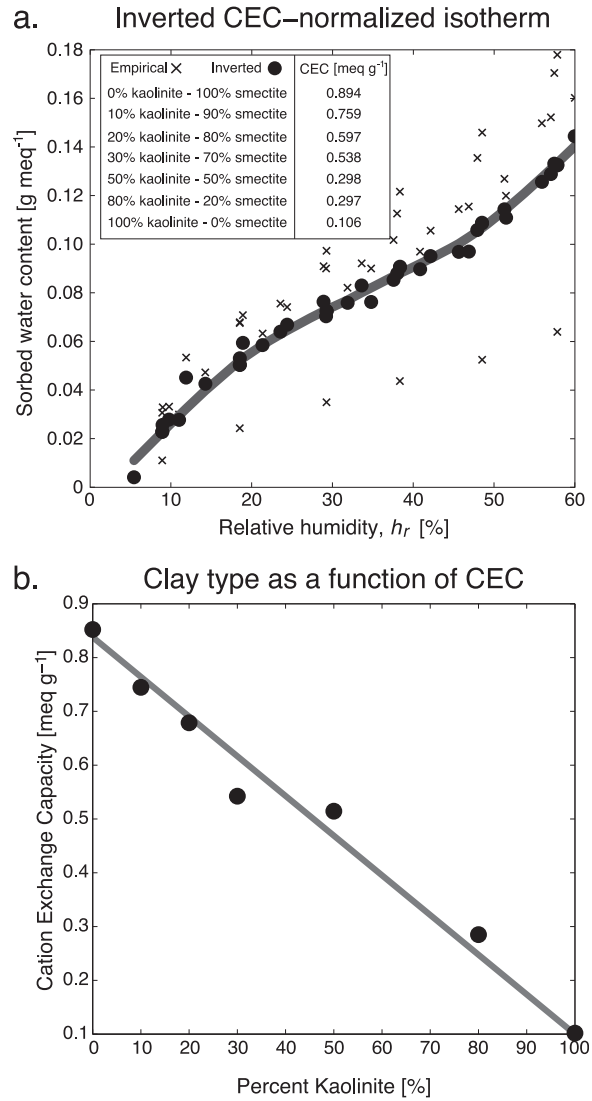


Figure 7. Inversion results. (a) Normalized desorption isotherm computed from the mean CEC value of the posterior distributions obtained from the inversion. The normalized water content in all clay mixtures is shown collectively as filled circles, and the raw values are shown collectively as crosses. The inverted CEC values are also shown. (b) A linear relationship between the CEC and the clay content (in weight) was observed from the inverted CEC. This is consistent with equation (1) of the main text. Data from *Likos and Lu* [2002].

(14)) is dependent on the position in the wetting/drying loop. The respective $\bar{\xi}$ values were comprised between 11.9 and 6.9 (dimensionless) for adsorption and desorption data, respectively. This corresponds to a difference in sorption heats $\Delta E = RT \ln C$ on the order of 1 to 5 kJ mol⁻¹, which is consistent with values reported in the literature (refer to the data sources in Tables 1 and 2; inverted values are provided in Tables 3 and 4). Note that this narrow range of sorption energies comprises a diverse set of clay mineralogies; hence, at first order, water sorption is generally independent of the crystalline plane (sorption heats are the same for all

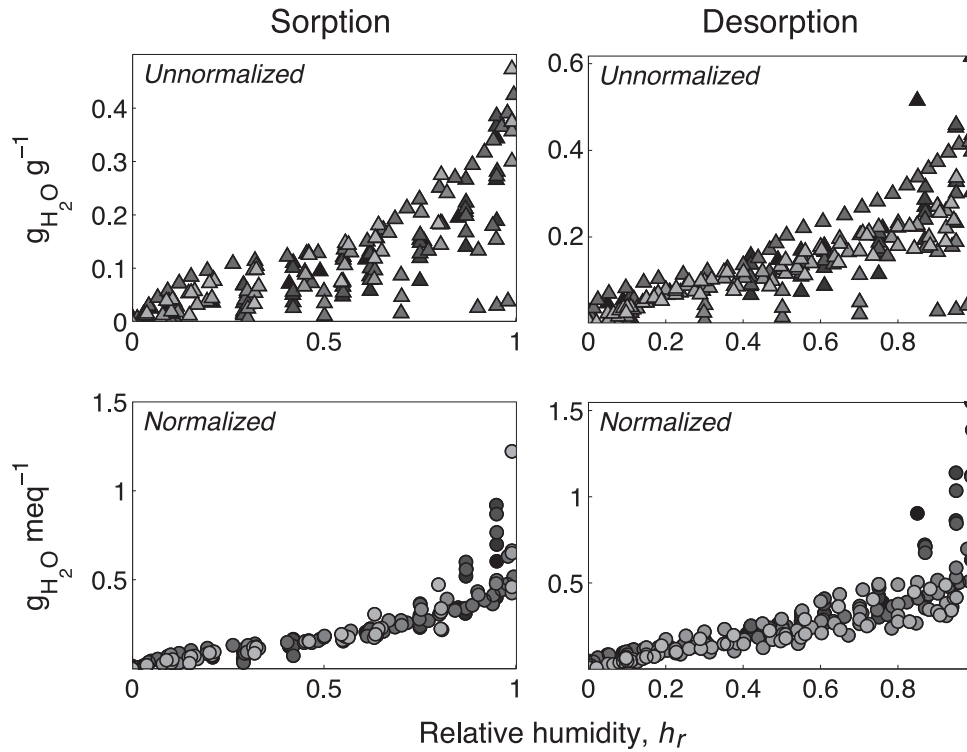


Figure 8. Plots of all data points used to invert the normalized cation exchange capacity $\overline{\text{CEC}}_i$. The raw data (triangles, upper figures) show significantly more scatter than the $\overline{\text{CEC}}_i$ -normalized data plots (circles, bottom circles). Both adsorption (right side) and desorption data (left side) sets are used here. See Table 1 for data sources.

surface sites including external and interlayer sites for 2:1 clays).

[28] In the present formulation, the bound water parameter is closely related to the monolayer water content for desorption data, and cannot be accurately constrained without determining v_m from the adsorption data as input in the desorption analysis. In the absence of adsorption data, the sum $v_m + bw$ can be used as a proxy for v_m , as long as it is recognized that some component of irreducible water is accounted for in this measure. Values for clay bound water bw are provided in Table 4. The optimal $\overline{\text{CEC}}_i$ -normalized monolayer water content determined from this analysis is on the order of $bw \approx 100$ mg of water per gram of clay.

[29] From equation (16) we can determine the critical relative humidity at which the first equivalent monolayer is filled ($v_m = v$). We obtain a second-order polynomial and the positive root of this polynomial yields

$$h_r(v = v_m) = \frac{\sqrt{C} - 1}{C - 1}, \quad (24)$$

with $C = (1 - \bar{\xi}\bar{v}_m)^{-1}$. Taking $\bar{\xi} = 6.9$ meq g⁻¹ and $\bar{v}_m = 0.08$ g meq⁻¹, we obtain a critical relative humidity of approximately 0.40 correlated to the inflection point of the sigmoidal adsorption isotherm (Figures 10 and 11). This is in fair agreement with Newman [1983] who found that a complete monolayer of water is obtained at a mean relative humidity of 0.47 for 58 British soils. In the case of Na-montmorillonite, Cases *et al.* [1997] showed that at

room relative humidity (around 40%), their sample still contained 50% dehydrated layers, which indeed corresponds to one fully saturated layer of water in our model. Using the same approach as above, it is easy to find the critical relative humidity at which the second equivalent hydration layer is fully saturated. This yields

$$h_r(v = 2v_m) = \frac{C - 4 + \sqrt{C^2 + 8C}}{4(C - 1)}. \quad (25)$$

Taking $\bar{\xi} = 6.9$ meq g⁻¹ and $\bar{v}_m = 0.08$ g meq⁻¹, we obtain a critical relative humidity of approximately 0.61, which is in excellent agreement with what is shown in Figures 5 and 9b. Note that the concept of having one or two homogeneous hydration layers is fictitious if we believe that, in reality, the water molecules are mainly located around the cation surface sites. We will discuss the number of water molecules per cation surface site in section 4.

3.3. Model Limitation

[30] It is always interesting and instructive to find a data set for which our model does not work, because it does not correctly account for the discrimination between a monolayer hydration state, bilayer hydration state, and pore water sorption. Michot *et al.* [2005] reported sorption/desorption isotherms for four samples of synthetic Na-vermiculite, which belongs to the smectite group. The cation exchange capacity of the samples are not reported by Michot *et al.* [2005], but Lipsicas [1984] gave a CEC for vermiculite

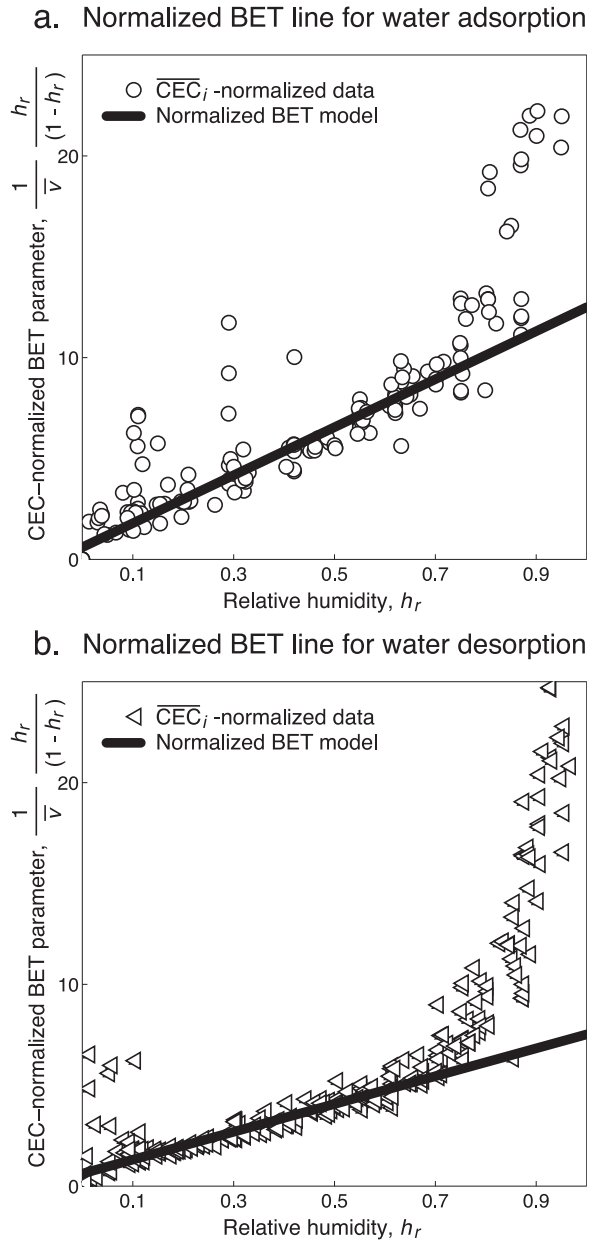


Figure 9. Resulting fit of the \overline{CEC}_i -scaled BET parameter space. (a) Adsorption trend. (b) Desorption trend. See Table 1 for data sources. The departure from the linear trends at high values of the relative humidity represents the transition from the hygroscopic and capillary waters. Correlation values of 0.79 and 0.93 for adsorption and desorption, respectively, for $h_r[0.1\ 0.61]$.

of $1.8\ \text{meq g}^{-1}$. Taking $\delta(\text{Na}) = 0.5$. We obtain $\overline{CEC}(\text{Na}) = 0.8\ \text{meq g}^{-1}$ and can now predict the amount of sorbed water on the surface of vermiculite as a function of the relative humidity, using the BET equation scaled with $\overline{CEC}(\text{Na}) = 0.8\ \text{meq g}^{-1}$. The measured versus predicted amounts of water sorbed on the mineral surface are shown in Figure 11. Clearly, the BET equation is unable to reproduce the clay-water sorption isotherm for these samples, especially at low relative humidities. The scaling proposed in the present paper could be applied to a more sophisticated sorption/desorption model accounting for discrimination between monolayer and

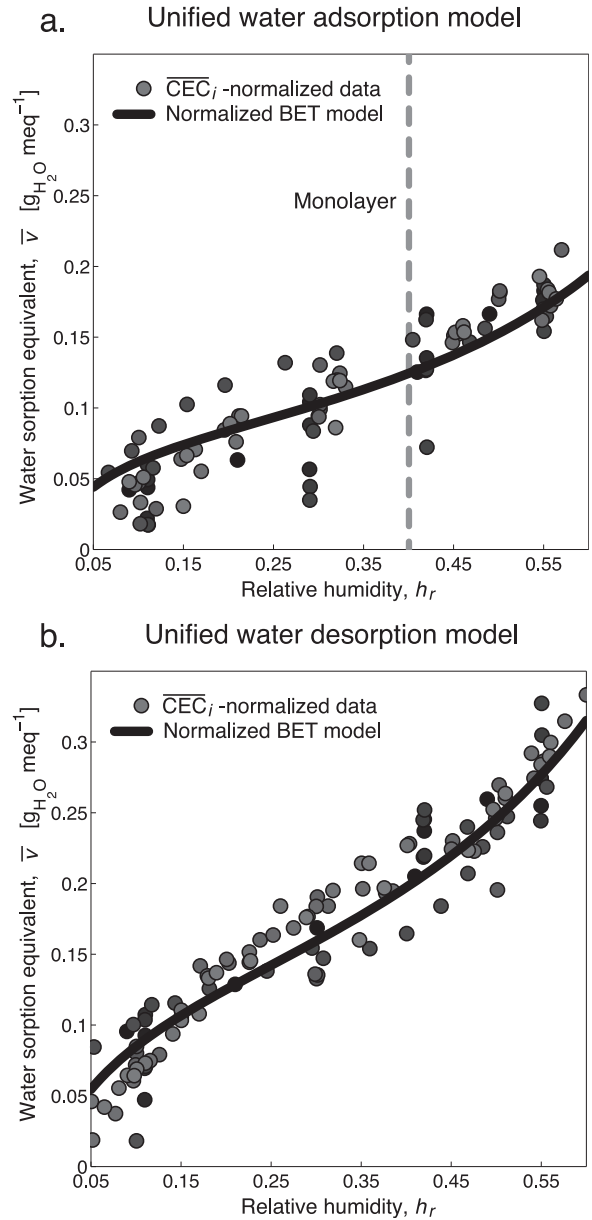


Figure 10. Resulting fit of the normalized sorption model to the normalized data set, see equation (20), using \overline{CEC}_i in place of the CEC. (a) Adsorption master curve isotherms. The point at which the first monolayer (corresponding to $\bar{v}_m = 0.08\ \text{g meq}^{-1}$) is filled is also shown. (b) Desorption master curve isotherms. See Table 1 for data sources. Correlation values of 0.94 and 0.92 were calculated for adsorption and desorption, respectively, for $h_r[0.1\ 0.61]$.

bilayer hydration state and interlayer versus external sorption [Laird, 1999; Michot et al., 2005; Ferrage et al., 2010].

3.4. Influence of Temperature

[31] Here we briefly discuss the effect of temperature at standard conditions (10–30°C). Using the scaled BET equation, the influence of temperature is explicitly described as

$$\frac{1}{\bar{v}} \left(\frac{h_r}{1-h_r} \right) = \frac{1}{\bar{v}_m} + \bar{\xi}(T)(h_r - 1), \quad (26)$$

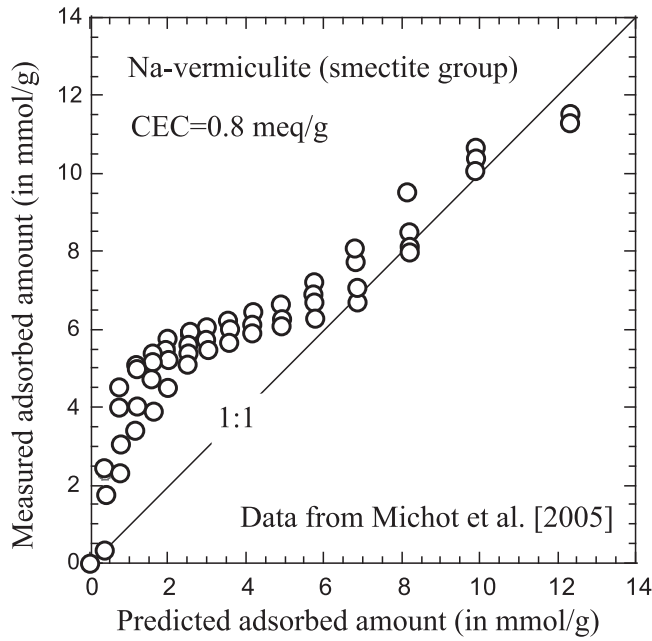


Figure 11. Measured versus predicted water sorption on four samples of vermiculite. Our model clearly underpredicts the sorption of water at low relative humidities.

$$\bar{\xi}(T)\bar{v}_m = \frac{\exp\left(\frac{\Delta E}{RT}\right) - 1}{\exp\left(\frac{\Delta E}{RT}\right)}. \quad (27)$$

For the temperature range 10–30°C, the relative change of $\bar{\xi}(T)\bar{v}_m$ is very small. For ΔE ranging from 1 to 4 kJ, the relative variation of $\bar{\xi}(T)\bar{v}_m$ is between 2.6% to 5.0% in

this temperature range. Therefore, our earlier assumption to neglect the temperature effect for datasets taken in the temperature range 20–30°C is well justified.

4. Discussion

[32] We will first discuss the number of molecules of water per site. The number of water molecules is per cation exchange site is given by

$$\bar{N}_w = \frac{ve}{CECM_w} = \frac{\bar{v}e}{M_w}. \quad (28)$$

When the first hydration layer is saturated ($\bar{v} = \bar{v}_m$), we obtain an amount of 4.4 water molecules per cation site from equation (28), a result consistent with the work by Michot *et al.* [2005] (4 ± 1 water molecules per Na^+ site for four synthetic Na saponites). When the second layer of water molecules is filled, we have $\bar{v} = 2\bar{v}_m$. From equation (28), we obtain 8.8 water molecules per site using the normalized CEC. For a specific ion i , this water has to be divided by δ_i . For instance, for Mg^{2+} we have $\delta(\text{Mg}) = 0.6$; therefore, we obtain 15 water molecules per cation sites. This value can be compared with the value obtained by Laird [1999] for some Mg-saturated 2:1 phyllosilicates: 24 water molecules per surface site. From an independent approach, Henry and Bourlange [2004] obtained 12 bound water molecules per cation exchange site for clay-rich sedimentary rocks. A value of 15 bound water molecules per surface site has been proposed for smectite from theoretical considerations by Ransom and Helgeson [1994]. This distribution of values also masks the fact that hydration heterogeneity in smectites has been reported systematically in the literature. Indeed, Laird [1999] showed that all the layers are not similarly hydrated, with smaller hydration numbers for the interlayer sites than for the external cation exchange sites.

Table 3. Inversion Results for Adsorption Isotherms^a

Clay Type	CEC (meq g ⁻¹)	$\overline{\text{CEC}}_i$ (meq g ⁻¹)	σ (-)	δ^{-1} (-)	v_m (g g ⁻¹)	ΔE (kJ mol ⁻¹)
Ca-Montmorillonite ^b	1.053	0.790	0.021	1.33	0.063	3.5
Cu-Montmorillonite	–	0.475	0.022	–	0.038	1.5
Fe-Montmorillonite	–	0.664	0.009	–	0.053	2.5
Li-Montmorillonite ^b	2.017	0.847	0.014	2.38	0.068	4.1
Mg-Montmorillonite ^b	1.636	0.900	0.025	1.82	0.072	4.8
Na-Montmorillonite	–	0.465	0.015	–	0.037	1.4
Shale-A (Na) ^c	0.095	0.065	0.016	1.5	0.005	0.2
Shale-C (Na) ^c	0.500	0.299	0.024	1.7	0.024	0.8
Shale-D (Na) ^c	0.250	0.177	0.026	1.4	0.014	0.5
Midway Shale (Na)	–	0.715	0.002	–	0.057	2.8
Bentonite (Al-Fe-Mg-Na-Ca-K)	–	0.543	0.014	–	0.043	1.8
Bentonite (Ti-Al-Fe-Mn-Mg-Ca-Na-K-P)	–	0.520	0.008	–	0.042	1.7
Ca-Bentonite ^b	0.945	0.737	0.019	1.28	0.059	3.0
K-Bentonite	–	0.287	0.038	–	0.023	0.8
Li-Bentonite ^b	0.977	0.381	0.024	2.56	0.030	1.1
Mg-Bentonite ^b	1.041	0.635	0.023	1.64	0.051	2.3
Na-Bentonite	–	0.483	0.039	–	0.039	1.5
Raw-Bentonite (Na/Ca)	–	0.375	0.038	–	0.030	1.1
Saponite (Al-Mg-Na)	–	0.865	0.018	–	0.069	4.3

^aCEC estimates obtained by inversion of Ca, Li, Mg, and Na-clay subsets with a SD σ of the posterior probability distribution for the CEC. The scaling parameter δ_i^{-1} is determined from independently inverted $\overline{\text{CEC}}_i$ and CEC values. The monolayer concentrations v_m are calculated using the optimized $\overline{\text{CEC}}_i$ -scaled concentration $\bar{v}_m = 0.08 \text{ g meq}^{-1}$ and the following value of the slope parameter $\xi = 11.9 \text{ meq g}^{-1}$. The difference in desorption energies ΔE is calculated from the scaled BET slope parameter at 25°C.

^bCa-, Mg-, and Li-exchanged clays used in section 3.3.

^cNa-exchanged clays used in section 3.1.

Table 4. Inversion Results for Desorption Isotherms^a

Clay Type	CEC (meq g ⁻¹)	$\overline{\text{CEC}}_i$ (meq g ⁻¹)	σ (-)	δ^{-1} (-)	v_m (g g ⁻¹)	bw (g g ⁻¹)	ΔE (kJ mol ⁻¹)
Wy. mont. (Na) ^b	0.996	0.540	0.021	1.8	0.043	0.029	1.7
Wy. smectite, SWy-1 (Na) ^b	0.820	0.455	0.022	1.8	0.036	0.024	1.3
Wy. mont., Clay Spur (Na) ^b	0.950	0.557	0.009	1.7	0.045	0.030	1.8
MX-80 Bentonite, Wyoming (Na) ^b	0.760	0.510	0.014	1.5	0.041	0.027	1.6
Nat. Volclay, Wy. bentonite (Ca-Mg-Na) ^b	0.900	0.557	0.025	1.6	0.045	0.030	1.8
Nat. Volclay, Wy. bentonite (Na) ^b	0.900	0.545	0.015	1.7	0.044	0.029	1.7
Shale-A (Na) ^b	0.095	0.065	0.016	1.5	0.005	0.003	0.2
Shale-C (Na) ^b	0.500	0.299	0.024	1.7	0.024	0.016	0.8
Shale-D (Na) ^b	0.250	0.177	0.026	1.4	0.014	0.009	0.4
100% Smectite (Na) ^b	0.900	0.370	0.002	2.4	0.030	0.020	1.0
100% Kaolinite (Na) ^b	0.100	0.050	0.014	2.0	0.004	0.003	0.1
10/90 Kaolinite-Smectite (Na) ^b	0.622	0.336	0.008	1.9	0.027	0.018	0.9
20/80 Kaolinite-Smectite (Na) ^b	0.564	0.286	0.012	2.0	0.023	0.015	0.8
30/70 Kaolinite-Smectite (Na) ^b	0.506	0.256	0.012	2.0	0.020	0.014	0.7
50/50 Kaolinite-Smectite (Na) ^b	0.390	0.234	0.011	1.7	0.019	0.012	0.6
80/20 Kaolinite-Smectite (Na) ^b	0.216	0.121	0.015	1.8	0.010	0.006	0.3
Bentonite (Al-Fe-Mg-Na-Ca-K)	–	0.543	0.015	–	0.043	0.029	1.7
Bentonite (Ti-Al-Fe-Mn-Mg-Ca-Na-K-P)	–	0.520	0.019	–	0.042	0.028	1.6
Ca-Bentonite	–	0.737	0.008	–	0.059	0.039	2.8
K-Bentonite	–	0.287	0.002	–	0.023	0.015	0.8
Li-Bentonite	–	0.381	0.009	–	0.030	0.020	1.1
Mg-Bentonite	–	0.635	0.008	–	0.051	0.034	2.2
Na-Bentonite	–	0.483	0.009	–	0.039	0.026	1.5
Raw-Bentonite (Na/Ca)	–	0.375	0.005	–	0.030	0.020	1.0
Sapponite (Al-Mg-Na)	–	0.865	0.003	–	0.069	0.046	3.9
Soil-716	–	0.080	0.004	–	0.006	0.004	0.2

^aCEC estimates obtained from the inversion of Na-clay subsets with a SD σ of the posterior PDF for the CEC. The value of the scaling parameter δ_i^{-1} is determined from independently inverted $\overline{\text{CEC}}_i$ and CEC values. The monolayer concentrations v_m are calculated using the optimized $\overline{\text{CEC}}_i$ -scaled concentration $\bar{v}_m = 0.08 \text{ g meq}^{-1}$ and the following value of the slope parameter $\xi = 6.9 \text{ meq g}^{-1}$. The estimates for clay bound water bw are determined from the optimized value $\Gamma = 0.053$. The difference in desorption energies ΔE is calculated from the scaled BET slope parameter at 25°C.

^bNa-exchanged clays used in section 3.1.

[33] We now discuss the advantages of using the CEC rather than the specific surface area to normalize clay-water isotherms. Our first motivation is that the CEC is the key parameter used in the transport equations developed by *Revil et al.* [2011] in clayey materials. If we want to generalize this transport model to the unsaturated case, it is important to show that very few parameters are needed to characterize transport properties in unsaturated conditions. In the introduction, we briefly discussed how isotherms based on the specific surface area assume a uniform distribution of the water on the mineral surface. Because of the clustering of water molecules around cation surface sites, the CEC seems to be a better surrogate to predict clay-water sorption isotherms. Another advantage is that the CEC can account for the ionic composition of the pore water, which can be sorbed in the Stern layer, enabling the calculation of the effect of these cations upon the clay-water sorption isotherm. Hence, the model developed in this paper is promising as a simple, first-order approach to predict clay-water sorption isotherms in clayey materials.

[34] Finally, all analyses presented here refer to mono-ionic clays. In realistic geochemical conditions, clay sediments and shales are heteroionic and the pore water is a multicomponent solution with various concentrations of cations. *Leroy et al.* [2007] have developed an original approach based on Donnan equilibria and triple layer concepts to compute the sorption of cations on the surface of clay minerals for any pore water composition and mineral types. Their approach could be used to estimate relevant CEC values to properly scale the clay-water isotherms in our model.

5. Concluding Statements

[35] A model for clay-water isotherms has been presented. This model is based on the normalization of sorption isotherms by the CEC of the clay fraction accounting for the type of counterions located at the surface of the clay minerals. Only ions with large ionic potentials (Li^+ , Na^+ , Mg^{2+} , Ca^{2+}) have been tested in this work. It will be interesting for future analysis to use clays exchanged with larger ions having small ionic potentials (e.g., K^+), which do not show significant interlayer hydration. A comparison with the data set by *Michot et al.* [2005] shows some limitations of the present approach. However, the key concepts of the present paper (normalization by the CEC and by the type of counterions) could be applied to another isotherm model, which would be more general than the BET model.

[36] We plan to combine this model with a description of the capillary pressure curve to produce generalized capillary pressure curve for clay materials. This model will be coupled with a general model of cross-coupled flows in unsaturated clayey media extending the recent modeling effort made by *Revil et al.* [2011], which is itself based on unifying the transport properties of clay media using the CEC as a key parameter.

Appendix A: Sequential Inversion Strategy

[37] Two Bayesian analyses were performed in series to obtain independent probabilistic frameworks for the sorption and desorption models upon which the normalized

sorption model was built. The first step in the sequence implements an MCMC algorithm to determine the normalized \overline{CEC}_i , followed by strict Bayesian analysis of the normalized isotherm model (equation (19)) to determine the following parameters \bar{v}_m , Γ (for the inversion of the drying curve), and $\bar{\xi}$.

[38] The chosen variant of the MCMC algorithm [Haario *et al.* 2001; Tamminen, 2004] utilizes a memory mechanism based on a recursive update of the model variance known as the adaptive metropolis algorithm (AMA). This approach is used to compute the posterior probability density function (PDF) of the model parameters (in our case \overline{CEC}_i). This PDF is taken as Gaussian distributed. The PDF is defined from the stochastic sampling of the parameter space once the model variance σ has been minimized after running a number of realizations. This process is strictly data driven. No model bias has been introduced in this step. Generalized CEC values are used to constrain the inversion a priori using the additional constraint $CEC_K < CEC_I < CEC_S$ (where the subscripts indicate the clay type, e.g., S for smectite) using values ranging from 0.001 to 1 meq g⁻¹ (see Figure 1). Clays for which we have both sorption and desorption data samples the same value for \overline{CEC}_i is used for both sorption and desorption during each realization. Although, according to our model, we are specifically inverting for \overline{CEC}_i in this step, actual estimates of the CEC are used as prior constraints to assign higher likelihood to models in which \overline{CEC}_i approaches CEC. The misfit is defined by the RMS error associated with the resulting scatter of the \overline{CEC}_i -normalized data, and the posterior likelihood is defined according to the joint probability of the data and model PDFs. The results of this step are presented in Figure 8.

[39] To optimize the normalized isotherm, a Bayesian analysis of the parameter space was performed within the following given bounds, $\bar{v}_m \in [0.001; 0.1]$; $\Gamma \in [0.001; 0.1]$, and $\bar{\xi} \in [0.1; 20]$. A posterior PDF is computed first for the \overline{CEC}_i -normalized adsorption data to determine the scaled monolayer parameter \bar{v}_m and the normalized sorption constant $\bar{\xi}$. The parameters are again taken as Gaussian distributed, and the posterior likelihood is determined from the misfit of the computed normalized BET line and the normalized data, using equation (19) as the kernel with Γ fixed at 0. For the desorption isotherms, the value of \bar{v}_m is input from the previous step, and Γ is optimized following a similar procedure. These results are shown in Figure 9. The normalized model presented in Figure 10 is calculated with the values of \overline{CEC}_i , \bar{v}_m , Γ , and $\bar{\xi}$ determined from this sequential inversion using the \overline{CEC}_i -scaled variant of equation (17). Correlation coefficients were obtained for both \overline{CEC}_i -normalized sorption data, as well as the transformed data in BET parameter space, indicating a near linear correlation of the scaled sorption data to the predicted values shown in Figures 9 and 10. Correlation values of 0.94, 0.92 were calculated for \overline{CEC}_i -normalized adsorption and desorption data, as well as 0.79 and 0.93 for \overline{CEC}_i -normalized BET lines, respectively (a correlation value of 1 corresponds to a perfectly linear trend).

[40] The mineralogical parameter δ_i can only be obtained empirically from the data when the true CEC of the samples are known; further inquiry is required to better constrain this parameter. However, estimates of the monolayer

water volume and the bound water can be made by simply multiplying the scaled parameters by the scaled CEC, $v_m = \bar{v}_m \overline{CEC}_i$, and $bw = \Gamma \overline{CEC}_i$.

[41] **Acknowledgments.** We thank the Office of Science (BER), US Department of Energy (award DE-FG02-08ER646559) for financial support. We thank James T. Krushin for fruitful discussions. We also thank the Associate Editor and three anonymous referees for their very constructive comments and the time they have invested in our manuscript.

References

- Aochi, Y., and W. Farmer (2010), Effects of surface charge and particle morphology on the sorption/desorption behavior of water on clay minerals, *Colloids Surf. A: Physicochem. Eng. Aspects*, 374, 22–32, doi:10.1016/j.colsurfa.2010.10.039.
- Avena, M. J., and C. P. De Pauli (1998), Proton adsorption and electrokinetics of an Argentinean Montmorillonite, *J. Colloid Interface Sci.*, 202, 195–204.
- Banin, A., and A. Amiel (1970), A correlative study of the chemical and physical properties of a group of natural soils of Israel, *Geoderma*, 3, 185–198.
- Bérend, I., J. M. Cases, M. François, J. P. Uriot, L. J. Michot, A. Masion, and F. Thomas (1995), Mechanism of adsorption and desorption of water vapour by homoionic montmorillonites: 2. The Li⁺, Na⁺, K⁺, Rb⁺ and Cs⁺ exchanged forms, *Clays Clay Miner.*, 43, 324–336.
- Broekhoff, J., and J. D. Boer (1967a), Studies on pore systems in catalysts: x calculations of pore distributions from the adsorption branch of nitrogen sorption isotherms in the case of open cylindrical pores A: Fundamental equations, *J. Catal.*, 9, 8–15.
- Broekhoff, J., and J. D. Boer (1967b), Studies on pore systems in catalysts: x calculations of pore distributions from the adsorption branch of nitrogen sorption isotherms in the case of open cylindrical pores B: Applications, *J. Catal.*, 9, 15–27.
- Brunauer, S., P. Emmett, and E. Teller (1938), Adsorption of gases in multimolecular layers, *J. Am. Chem. Soc.*, 60, 309–319.
- Cancela, G., F. Huertas, E. R. Taboada, F. Sánchez-Rasero, and H. Laguna (1997), Adsorption of water vapor by homoionic montmorillonites. Heats of adsorption and desorption, *J. Colloid Interface Sci.*, 185, CS 964572, 343–354.
- Carroll, D. (1959), Ion exchange in clays and other minerals, *Geol. Soc. Am. Bull.*, 70(6), 749–780.
- Cases, J. M., I. Bérend, M. François, J. P. Uriot, L. J. Michot, and F. Thomas (1997), Mechanism of adsorption and desorption of water vapour by homoionic montmorillonite: 3. The Mg²⁺, Ca²⁺, Sr²⁺ and Ba²⁺ exchanged forms, *Clays Clay Miner.*, 45, 8–22.
- Chemkhi, S., F. Zagrouba, and A. Ballagi (2004), Thermodynamics of water sorption in clay, *Desalination*, 166, 393–399, doi:10.1016/j.desal.2004.06.094.
- Conin, M., P. Henry, S. Bourlange, H. Raimbourg, and T. Reuschlé (2011), Interpretation of porosity and LWD resistivity from the Nankai accretionary wedge in light of clay physicochemical properties: Evidence for erosion and local overpressuring, *Geochem. Geophys. Geosyst.*, 12, 1–17, Q0AD07, doi:10.1029/2010GC003381.
- Delay, J., and M. Distinguin (2004), Hydrogeological investigations in deep wells at the meuse/haute marne underground research laboratory, in *Engineering Geology for Infrastructure Planning in Europe*, Lecture Notes in Earth Sciences, Vol. 104, edited by R. Hack, R. Azzam, and R. Charlier, pp. 219–225, Springer, New York.
- Dontsova, K. M., L. Norton, C. Johnston, and J. Bigham (2004), Influence of exchangeable cations on water adsorption by soil clays, *Soil Sci. Soc. Am. J.*, 68, 1218–1227.
- Ferrage, E., B. Lanson, B. A. Sakharov, and V. A. Drits (2005), Investigation of smectite hydration properties by modeling of X-ray diffraction profiles. Part 1. Montmorillonite hydration properties, *Am. Mineralog.*, 90, 1358–1374.
- Ferrage, E., B. Lanson, L. J. Michot, and J.-L. Robert (2010), Hydration properties and interlayer organization of water and ions in synthetic N-smectite with tetrahedral layer charge. Part 1. Results from X-ray diffraction profile modeling, *J. Phys. Chem. C*, 114, 4515–4526.
- Furmaniak, S., A. Terzyk, P. Gauden, and G. Rychlicki (2005), Parameterization of the corrected Dubinin-Serpinsky adsorption isotherm equation, *J. Colloid Interface Sci.*, 291, 600–605, doi:10.1016/j.jcis.2005.07.062.
- Gauden, P. (2005), Does the Dubinin-Serpinsky theory adequately describe water adsorption on adsorbents with high-energy centers?, *J. Colloid Interface Sci.*, 282, 249–260, doi:10.1016/j.jcis.2004.08.091.

- Haario, H., E. Saksman, and J. Tamminen (2001), An adaptive metropolis algorithm, *Bernoulli*, *7*, 223–242, doi:10.2307/3318737.
- Henry, P., and S. Bourlange (2004), Smectite and fluid budget at Nankai IODP sites derived from cation exchange capacity, *Earth Planet. Sci. Lett.*, *219*, 129–145, doi:10.1016/S0012-821X(03)00694-0.
- Jougnot, D., A. Revil, N. Lu, and A. Wayllace (2010), Transport properties of the Callovo-Oxfordian clay rock under partially-saturated conditions, *Water Resour. Res.*, *46*, W08514, doi:10.1029/2009WR008552.
- Kowalczyk, P., M. Jaroniec, A. P. Terzyk, K. Kaneko, and D. D. Do (2005), Improvement of the Derjaguin-Broekhoff-de Boer theory for capillary condensation/evaporation of nitrogen in mesoporous systems and its implications for pore size analysis of MCM-41 silicas and related materials, *Langmuir*, *21*(5), 1827–1833, doi:10.1021/la047645n.
- Krushin, J. (2005), Quantifying shale porosity—A thermodynamically based, predictive model which includes the effects of mechanical compaction, temperature, mineralogy, and chemical diagenesis, *Gulf Coast Assoc. Geo. Soc. Trans.*, *55*, 401–414.
- Laird, D. A. (1999), Layer charge influences on the hydration of expandable 2:1 phyllosilicates, *Clays Clay Miner.*, *47*, 630–636.
- Leroy, P., and A. Revil (2009), Spectral induced polarization of clays and clay-rocks, *J. Geophys. Res.*, *114*, B10202, doi:10.1029/2008JB006114.
- Leroy, P., A. Revil, S. Altmann, and C. Tournassat (2007), Modeling the composition of the pore water in a clay-rock geological formation (Callovo-Oxfordian, France), *Geochim. Cosmochim. Acta*, *71*(5), 1087–1097, doi:10.1016/j.gca.2006.11.009.
- Likos, W., and N. Lu (2002), Water vapor sorption behavior of smectite-kaolinite mixtures, *Clays Clay Miner.*, *50*(5), 553–561.
- Limousin, G., J.-P. Goulet, L. Charlet, S. Szenknect, V. Barthès, and M. Krimissa (2007), Sorption isotherms: A review on physical bases, modeling and measurement, *Appl. Geochem.*, *22*, 249–275, doi:10.1016/j.apgeochem.2006.09.010.
- Lipsicas, M. (1984), Molecular and surface interactions in clay intercalates, in *Physics and Chemistry of Porous Media*, edited by D. L. Johnson and P. N. Sen, pp. 191–202, American Institute of Physics, New York.
- Lockhart, N. C. (1980), Electrical properties and the surface characteristics and structure of clays, II, Kaolinite: A nonswelling clay, *J. Colloid Interface Sci.*, *74*, 520–529.
- Ma, C., and R. A. Eggleton (1999), Cation exchange capacity of kaolinite, *Clays Clay Miner.*, *47*, 174–180.
- Malikova, N., A. Cadene, E. Dubois, V. Marry, S. Durand-Vidal, P. Turq, J. Breu, S. Longeville, and J. M. Zanotti (2007), Water diffusion in a synthetic hectorite clay studied by quasi-elastic neutron scattering, *J. Phys. Chem. C*, *111*, 17603–17611.
- Michot, L. J., I. Bihannic, M. Pelletier, E. Rinnert, and J.-L. Robert (2005), Hydration and swelling of synthetic Na-saponites: Influence of layer charge, *Am. Mineralog.*, *90*(1), 166–172.
- Middleton, G. (2003), *Encyclopedia of Sediments and Sedimentary Rocks*, 928 pp., Kluwer Academic, Dordrecht, The Netherlands.
- Mihoubi, D., and A. Bellagi (2006), Thermodynamic analysis of sorption isotherms of bentonite, *J. Chem. Thermodynam.*, *38*, 1105–1110, doi:10.1016/j.jct.2005.11.010.
- Mitchell, J. (1992), *Fundamentals of Soil Behavior*, 2nd ed., Wiley, New York.
- Mokrejš, P., A. Zikánová, D. Hradil, K. Štulík, V. Pacáková, M. Kočířik, and M. Eić (2005), The influence of heat pre-treatment on the sorption of water vapour on bentonite, *Adsorption*, *11*, 57–63.
- Montes-Hernandez, G., J. Duplay, L. Martinez, Y. Géraud, and B. Rousset-Tournier (2003), Influence of interlayer cations on the water sorption and swelling-shrinkage of MX80 bentonite, *Appl. Clay Sci.*, *23*, 309–321, doi:10.1016/S0169-1317(03)00130-3.
- Mooney, R., A. Keenan, and L. Wood (1952), Adsorption of water vapor by montmorillonite. I. Heat of desorption and application of BET theory, *J. Am. Chem. Soc.*, *74*(6), 1367–1371.
- Neimark, A., and P. Ravikovitch (2001), Capillary condensation in MMS and pore structure characterization, *Micropor. Mesopor. Mat.*, *44*(45), 697–707.
- Newman, A. (1983), The specific surface of soils determined by water sorption, *J. Soil Sci.*, *34*, 23–32.
- Patchett, J. G. (1975), An investigation of shale conductivity, Society of Professional Well Logging Analysis 16th Logging Symposium, Paper U, 41 p.
- Rabaute, A., A. Revil, and E. Brosse (2003), In situ mineralogy and permeability logs from downhole measurements: Application to a case study in chlorite-coated sandstones, *J. Geophys. Res.*, *108*(B9), 2414, doi:10.1029/2002JB002178.
- Ransom, B., and H. C. Helgeson (1994), A chemical and thermodynamic model of dioctahedral 2:1 layer clay minerals in diagenetic processes: Regular solution representation of interlayer dehydration in smectite, *Am. J. Sci.*, *294*, 449–484, doi:10.2475/ajs.294.4.449.
- Ravikovitch, P., and A. Neimark (2002), Density functional theory of adsorption in spherical cavities and pore size characterization of templated nanoporous silicas with cubic and three-dimensional hexagonal structures, *Langmuir*, *18*, 1550–1560.
- Revil, A., and P. Leroy (2004), Constitutive equations for ionic transport in porous shales, *J. Geophys. Res.*, *109*, B03208, doi:10.1029/2003JB002755.
- Revil, A., L. Cathles, S. Losh, and J. Nunn (1998), Electrical conductivity in shaly sands with geophysical applications, *J. Geophys. Res.*, *103*(B10), 23,295–23,936, doi:10.1029/98JB02125.
- Revil, A., W. Woodruff, and N. Lu (2011), Constitutive equations for coupled flows in porous media, *Water Resour. Res.*, *47*, W05548, doi:10.1029/2010WR010002.
- Rinnert, E., C. Carteret, B. Humbert, G. Fragneto-Cusani, J. Ramsay, A. Delville, J.-L. Robert, I. Bihannic, M. Pelletier, and L. Michot (2005), Hydration of a synthetic clay with tetrahedral charges: A multidisciplinary experimental and numerical study, *J. Phys. Chem. B*, *23*, 745–23,759, doi:10.1021/jp050957u.
- Rousseau-Gueutin, P., P. Gonçalves, M. Cruchaudet, G. de Marsily, and S. Violette (2010), Hydraulic and chemical pulse tests in a shut-in chamber imbedded in an argillaceous formation: Numerical and experimental approaches, *Water Resour. Res.*, *46*, W08516, doi:10.1029/2008WR007371.
- Saarenketo, T. (1998), Electrical properties of water in clay and silty soils, *J. Appl. Geophys.*, *40*, 73–88.
- Salles, F., J.-M. Douillard, R. Denoyel, O. Bildstein, M. Jullien, I. Beurroies, and H. VanDamme (2009), Hydration sequence of swelling clays: Evolutions of specific surface area and hydration energy, *J. Colloid Interface Sci.*, *333*, 510–522, doi:10.1016/j.jcis.2009.02.018.
- Sammartino, S., A. Bouchet, D. Prêt, J. Parneix, and E. Tevissen (2003), Spatial distribution of porosity and minerals in clay rocks from the callovo-oxfordian formation (Meuse/Haute-Marne, Eastern France)—Implications on ionic species diffusion and rock sorption capability, *Appl. Clay Sci.*, *23*, 157–166, doi:10.1016/S0169-1317(03)00098-X.
- Schneider, M., and K.-U. Goss (2011), Temperature dependence of the water retention curve for dry soils, *Water Resour. Res.*, *47*, W03506, doi:10.1029/2010WR009687.
- Shainberg, I., N. Alperovitch, and R. Keren (1988), Effect of magnesium on the hydraulic conductivity of Na-smectite-sand mixtures, *Clays Clay Miner.*, *36*, 432–438.
- Shang, S., R. Horne, and H. Ramey (1995), Water vapor adsorption on geothermal reservoir rocks, *Geothermics*, *24*(4), 523–540.
- Sinitsyn, V. A., S. U. Aja, D. A. Kulik, and S. A. Wood (2000), Acid-base surface chemistry and sorption of some lanthanides on K⁺-saturated Marblehead illite. I. Results of an experimental investigation, *Geochim. Cosmochim. Acta*, *64*, 185–194.
- Smith, C. W., A. Hadas, J. Dan, and H. Koyumdjisky (1985), Shrinkage and atterberg limits in relation to other properties of principal soil types in Israel, *Geoderma*, *35*(1), doi:10.1016/0016-7061(85)90055-2.
- Srodon, J., and D. McCarty (2008), Surface area and layer charge of smectite from CEC and EGME/H₂O-retention measurements, *Clays Clay Miner.*, *56*(2), 155–174, doi:10.1346/CCMN.2008.0560203.
- Stepkowska, E., J. Pérez-Rodríguez, C. Maqueda, and E. Starnawska (2004), Variability in water sorption and in particle thickness of standard smectites, *Appl. Clay Sci.*, *24*, 185–199, doi:10.1016/j.clay.2003.03.004.
- Su, Q., Q. Feng, and Z. Shang (2000), Electrical impedance variation with water saturation in rock, *Geophysics*, *65*, 68–75.
- Tamminen, J. (2004), Validation of nonlinear algorithms with Markov chain Monte Carlo method, *J. Geophys. Res.*, *109*(d19), D19303, 303, doi:10.1029/2004JD004927.
- Tuller, M., and D. Or (2005), Water films and scaling of soil characteristic curves at low water contents, *Water Resour. Res.*, *41*, W09403, doi:10.1029/2005WR004142.
- Vaudelet, P., A. Revil, M. Schmutz, M. Franceschi, and P. Bégasat (2011a), Induced polarization signatures of cations exhibiting differential sorption behaviors in saturated sands, *Water Resour. Res.*, *47*, W02526, doi:10.1029/2010WR009310.
- Vaudelet, P., A. Revil, M. Schmutz, M. Franceschi, and P. Bégasat (2011b), Changes in induced polarization associated with the sorption of sodium, lead, and zinc on silica sands, *J. Colloid Interface Sci.*, *360*, 739–752.

- Woodruff, W., A. Revil, A. Jardani, D. Nummedal, and S. Cumella (2010), Stochastic Bayesian inversion of borehole self-potential measurements, *Geophys. J. Int.*, 183, 748–764, doi:10.1111/j.1365-246X.2010.04770.x.
- Yukselen, Y., and A. Kaya (2006), Prediction of cation exchange capacity from soil index properties, *Clay Miner.*, 41, 827–837, doi:10.1180/0009855064140222.
- Yukselen-Askoy, Y., and A. Kaya (2010), Method dependency between specific surface area and soil physicochemical properties, *Appl. Clay Sci.*, 50(2), 182–190, doi:10.1016/j.clay.2010.07.020.
- Zundel, J. P., and B. Siffert (1985), Mécanisme de rétention de l'octylbenzène sulfonate de sodium sur les minéraux argileux, in *Solid-Liquid Interactions in Porous Media*, pp. 447–462, Technip, Paris.

A. Revil, ISTerre, CNRS, UMR CNRS 5275, Université de Savoie, F-73376 cedex, Le Bourget du Lac, France. (arevil@mines.edu)
W. F. Woodruff, Department of Geophysics, Colorado School of Mines, Green Center, 1500 Illinois Street, Golden, CO 80401, USA.